Çukurova Üniversitesi
Mühendislik Fakültesi Dergisi
Çukurova University
Journal of the Faculty of Engineering
ISSN: 2757-9255 CİLT/VOLUME: 39 SAYI/ISSUE: 3 EYLÜL/SEPTEMBER 2024

2-D Microstructure Modeling based on Micrographs of Laser Powder Bed Fusion Melted Specimens

Ali Can KAYA [1,a]

[1]*Turkish-German University, Faculty of Engineering, Department of Mechatronics Engineering, Istanbul, Türkiye*

[a]***ORCID**: 0000-0003-2856-5508*

Article Info
Received : 23.02.2024
Accepted : 27.09.2024
DOI: 10.21605/cukurovaumfd.1559938

Corresponding Author
Ali Can KAYA
alican.kaya@tau.edu.tr

Keywords
Microstructure
FE method
Additive manufacturing
Fusion boundary

***How to cite:** KAYA, A.C., (2024). 2-D Microstructure Modeling based on Micrographs of Laser Powder Bed Fusion Melted Specimens. Cukurova University, Journal of the Faculty of Engineering, 39(3), 609-615.*

ABSTRACT

2D microstructural modeling based on the optical micrographs was successfully carried out. Creating a realistic microstructural model containing microstructural features such as fusion boundaries and phases makes it possible to analyze the relationship between the microstructure and property. We implemented this method to the 316 stainless steel (SS) laser powder bed fusion melted specimens. The optical micrographs were meshed and imported into finite element (FE) software. According to the results, the orientation of the fusion boundaries significantly influenced the mechanical properties of the printed parts. Stress localization was significant when the fusion boundaries were parallel to the loading direction. The situation differed when the fusion boundaries were perpendicular to the loading direction. In this case, the large amount and size of fusion boundaries showed significant ductility with homogenously distributed straining.

Lazer Toz Yataklı Füzyon ile Eritilmiş Numunelerin Mikrograflarına Dayalı 2 Boyutlu Mikroyapı Modellemesi

Makale Bilgileri
Geliş : 23.02.2024
Kabul : 27.09.2024
DOI: 10.21605/cukurovaumfd.1559938

Sorumlu Yazar
Ali Can KAYA
alican.kaya@tau.edu.tr

Anahtar Kelimeler
Mikroyapı
Sonlu elemanlar metodu
İmalat
Füzyon sınırları

***Atıf şekli:** KAYA, A.C., (2024). 2-D Microstructure Modeling based on Micrographs of Laser Powder Bed Fusion Melted Specimens. Cukurova University, Journal of the Faculty of Engineering, 39(3), 609-615.*

ÖZ

Optik mikrograflara dayalı 2 boyutlu mikroyapısal modelleme başarıyla gerçekleştirildi. Füzyon sınırları ve fazlar gibi mikroyapısal özellikleri içeren gerçekçi bir mikroyapısal modelin oluşturulmasıyla mikroyapı ve özellik arasındaki ilişkinin analiz edilmesi mümkün olmuştur. Bu yöntemi 316 paslanmaz çelik (SS) lazer toz yataklı füzyon ile sinterlenmiş numunelere uyguladık. Optik mikrograflara mesh atıldı ve sonlu elemanlar (FE) yazılımına aktarıldı. Sonuçlara göre, füzyon sınırlarının yönelimi, 3d yazıcı ile üretilmiş parçaların mekanik özelliklerini önemli ölçüde etkilemektedir. Füzyon sınırları yükleme eksenine paralel olduğunda önemli bir gerilim lokalizasyonu oluşmuştur. Füzyon sınırları yükleme doğrultusuna dik olduğunda ise durum faklıdır. Bu durumda büyük miktarda ve boyuttaki füzyon sınırları, homojen olarak dağılmış bir şekil değiştirme ile önemli bir süneklik göstermiştir.

1. INTRODUCTION

Additive manufacturing technologies draw attention to part production for diverse applications. In additive manufacturing, various fabrication parameters, such as layer thickness, laser power, scanning speed, and hatching distance, influence the microstructure of the parts and result in a complex interplay between the microstructure and the mechanical properties. A substantial effort is dedicated to comprehending the impact of these production parameters on microstructure and mechanical properties [1].

The laser powder bed fusion process is an additive manufacturing method that uses a high-energy laser to melt metal powder layer by layer [2]. During this process, the laser impinged on a single point and tracked the surface of the powder bed. Melting of the powder results in a melt pool, which solidifies quickly and creates an anisotropic microstructure with elongated grains. Besides, melt pools intersect along the building direction and overlap with adjacent scan tracks, forming fusion boundaries between tracks and layers. Shifeng et al. [2] addressed that sharp corners were generated at the junction of layer-layer and track-track fusion boundaries, triggering crack initiation. They also discovered that slippage at these fusion boundaries enhanced material ductility, even under room-temperature loading conditions.

Several studies have investigated the impact of building direction, or texture, on mechanical properties [3-7]. For instance, Hitzler et al. [6] revealed maximum values for samples fabricated at a polar angle of 45 degrees. Contrary to that Guan et al. [3] illustrated that horizontally built 316L samples exhibited the highest tensile strength. Furthermore, Güden et al. [5] reported that strength increased with increasing the polar angle for 316L samples. As computational work, Ahmadi et al. [7] carried out a 3D numerical study on the effects of the microstructure on the mechanical properties of the parts fabricated by selective laser melting (SLM). They modeled the microstructure with grain and melt pools, simulated by overlapping cylinders interconnected by cohesive surfaces. They modeled the grains using the Voronoi tessellation method. Furthermore, Rodgers et al. [8] applied a computational method based on a Monte Carlo Potts model to generate an additively manufactured microstructure. Microstructure evolution was simulated using the melt pool shape, temperature gradient, and scan pattern.

To our knowledge, 2D microstructure modeling of laser powder bed fusion melted specimens based on optical micrographs has not been applied. Here in this study, FE modeling of the microstructure was conducted, and the influence of the fusion boundaries on the mechanical properties was elucidated.

2. MATERIALS AND METHODS

2.1. Materials

Specimens were produced using a laser powder bed fusion machine for additive manufacturing of metal parts (Concept Laser M2 Cusing, Concept Laser GmbH, Lichtenfels, Germany) [1]. The samples were synthesized with an energy density of 75 J mm^{-3} under a nitrogen gas atmosphere with the printing parameters in Table 1. The layer thickness of the parts was 30 µm.

Table 1. Printing parameters of the samples [1]

Parameters	Value
Laser power (W)	180
Spot size (µm)	140
Scann speed (mm/s)	700
Offset to original contour (mm)	0.0825
Hatching distance (mm)	0.115

Fig. 1 shows dogbone-shaped specimens of various sizes and shapes. The specimens were built vertically and parallel to the building directions. The thickness of the micros tensile specimens was 1 mm.

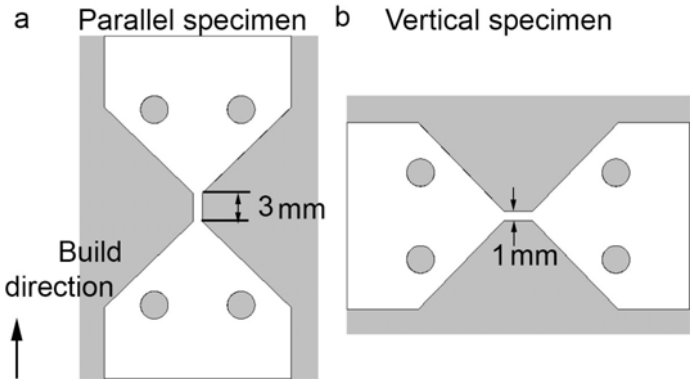

Figure 1. Dimension and shape of the a) parallel and b) vertical printed samples [1]

2.2. Metallographic Preparation

The etched samples were used to observe the microstructure optically. For this purpose, specimens were inserted in epoxy resin and ground on SiC abrasive paper with grit sizes spanning from 300 grit to 1200 grit. After that, polishing was conducted using diamond suspensions of 3 and 1 µm grain size for 5 and 3 min, respectively. Further polishing was accomplished with silica suspension for 1 minute.

To observe the fusion layers, etching was conducted with a V2A etchant at 50 ° C for 30 sec. The microstructure surface was then captured with a Leica DMRM light microscope (Leica Microsysteme Vertrieb GmbH, Wetzlar, Germany).

2.3. Image Processing

Before FE meshing, captured microstructure images were processed using a software, Image J [9]. Figure 2 demonstrates the image processing sequence. The optical micrograph was initially scaled, and then the ‘‘subtract background’’ tool was implemented to isolate the fusion boundaries. Secondly, the ‘‘make binary’’ tool was carried out to create a binary image. The emerging speckles in the background were removed using the ‘‘despeckle tool’’. Finally, the gray image value was inverted to develop the segmented fusion boundaries in the micrograph.

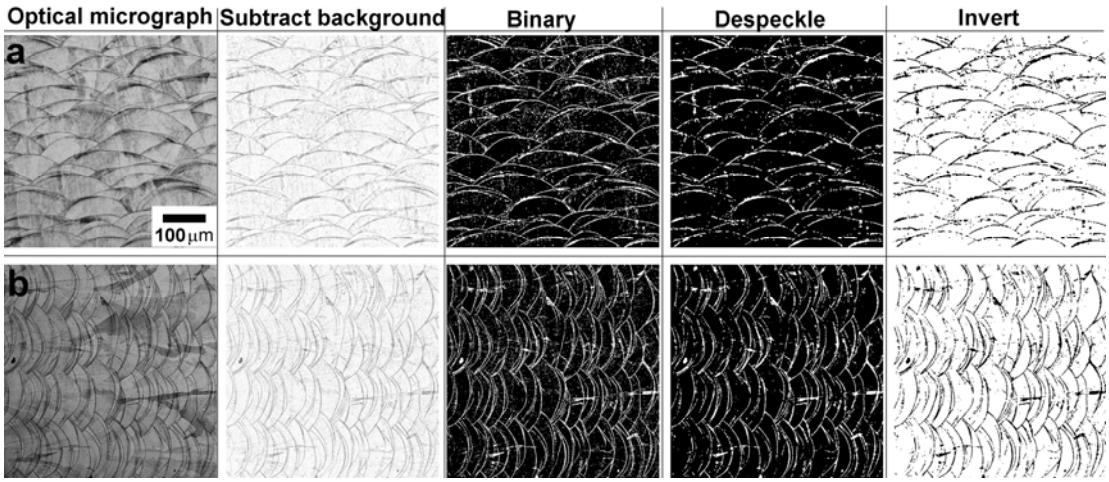

Figure 2. Image processing on the micrographs of the a) parallel and b) vertical specimens

2.4. FE Meshing

FE meshing was accomplished using the Im2mesh plug-in [10] based on MESH2D [11] (Delaunay mesh generator), which converted 2D multi-phase images into FE triangular meshes. The Im2mesh plug-in was executed in Matlab R2023a (The MathWorks Inc., Massachusetts, USA). Table 2 gives the parameters for meshing the microstructure.

Three essential parameters are used in the Im2mesh, including tolerance, hmax, and grad_limit. Tolerance is used as a tolerance for polygon simplification. hmax depicts the maximum mesh size. grad_limit explains the scalar gradient limit for the mesh [10, 11]. Generated meshes were recorded as .inp files and imported into the FE software.

Table 2. Parameters used for meshing

Parameters	Values
tolerance	1
hmax	2500
grad_limit	+0.25

2.5. FE Modeling

Initially, vertical and horizontally built microstructure meshes were scaled to their actual size using the copy command in FE Software. Fusion boundaries and matrix meshes were imported as different parts in the beginning. Then, those parts and nodes were merged only on the boundary. Constitutive material models were taken from our previous work [1]. Micro-tensile testing of the specimen was performed with a speed of 5 µm/s using a micro-testing machine (Kammrath und Weiss, Dortmund, Germany). Tensile testing was carried out under a digital light microscope to image the surface of the samples. Image series were acquired every 15 sec for evaluation in the digital image correlation method (DIC, Vic-2d, Correlated Solutions, Inc., Irmo, USA). Elongation of the printed samples was determined using a virtual extensometer function on the strain field. For more detailed information, please refer to reference [1]. The young modulus for horizontally and vertically built-up specimens were 193.3 GPa and 225 GPa, respectively. The yield strengths for horizontally and vertically built-up specimens were 513 and 667 MPa, respectively. Poisson's ratio was 0.3 [12]. The elastic-plastic material model was assigned to the matrix materials; however, only the elastic material model was set to the fusion boundaries. A 3-node linear plane stress triangle CPS3 with a linear geometric order was used as an element type. On one end, micrographs were fixed with encastre and displaced from the other end with a length of 0.016 mm, as illustrated in Fig. 3. The number of elements of vertically and horizontally built-up specimens was 101810 and 51511, respectively.

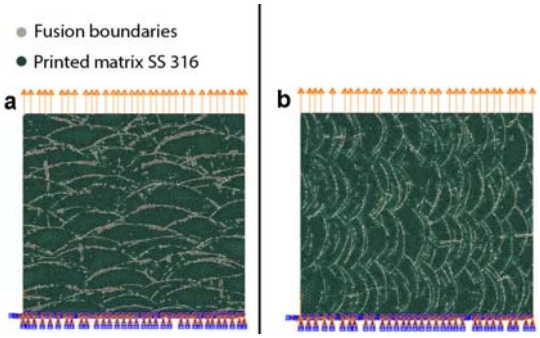

Figure 3. FE model of the printed a) parallel and b) vertical steel microstructures

2.6. XRD Measurement

XRD experiments were carried out on the printed sample using an XRD machine (Empyrean, Malvern Panalytical, Malvern, England) with Cu Kα radiation (λ = 1.54060 Å). XRD scans were carried out in the range of 2Θ = 40°–120°. Scan parameters include a step size of 0,013° and a holding time of 80 s per step.

3. RESULTS AND DISCUSSIONS

3.1. Microstructure Quantification

Parallel specimens have larger fusion boundary sizes than vertical specimens. The area percentage of the parallel specimen's fusion boundary is higher than that of the vertical specimen. The circularity and solidity

of both specimens are almost the same. The feret diameter of the fusion boundary was measured to be 8.9 and 14.6 µm for vertical and parallel specimens, respectively.

Table 3. Quantification of the fusion boundary of the printed specimens

Fusion boundary properties	Vertical specimen	Parallel specimen
Average size	21.4 µm	82 µm
Area percentage	12.3%	17.4%
Circularity	0.76	0.77
Solidity	0.82	0.82
Feret diameter	8.9 µm	14.6 µm

3.2. X-ray Diffraction

Fig. 4 illustrates the X-ray spectrum of the printed specimen. 316 stainless steel (SS) has an austenitic phase with ɣ-iron, also detected in the XRD.

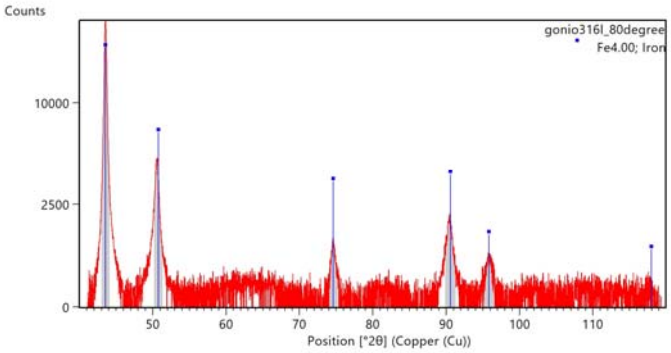

Figure 4. XRD Spectrum of the 316 steel sample fabricated by laser powder bed fusion

3.3. Effects of Fusion Boundary on the Mechanical Properties

Microtensile testing results were compared with the 2-D modeling results. The Mises stresses and displacement from the nodes at the side of the model were averaged and plotted in Fig. 5. The 2-D modeling results well matched with the elastic portion of the curve. In the plastic regime, however, there is a discrepancy between the vertical samples' modeling and micro tensile testing results. Interestingly, the plastic portion of the parallel specimen is consistent with the experimental results.

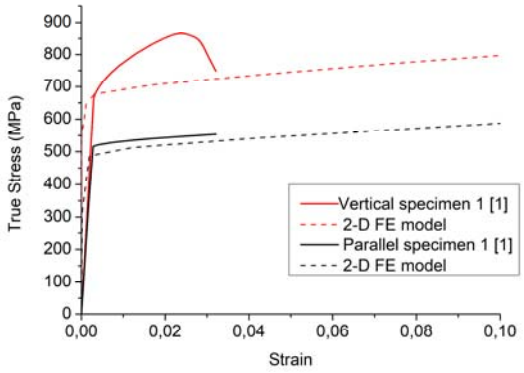

Figure 5. True stress-strain curves of the modeling results and micro tensile testing.

Mises stress and PEEQ strain fields of the vertical specimen was demonstrated in Fig. 6. At a strain of 0.02, stress concentrated on the fusion boundaries, and a large localized strain was observed in the microstructure. At a strain of 0.03, there is a significant elongation in the microstructure, resulting in a decrease in the stress. Localized strain is aligned with an angle of 45° to the loading axis.

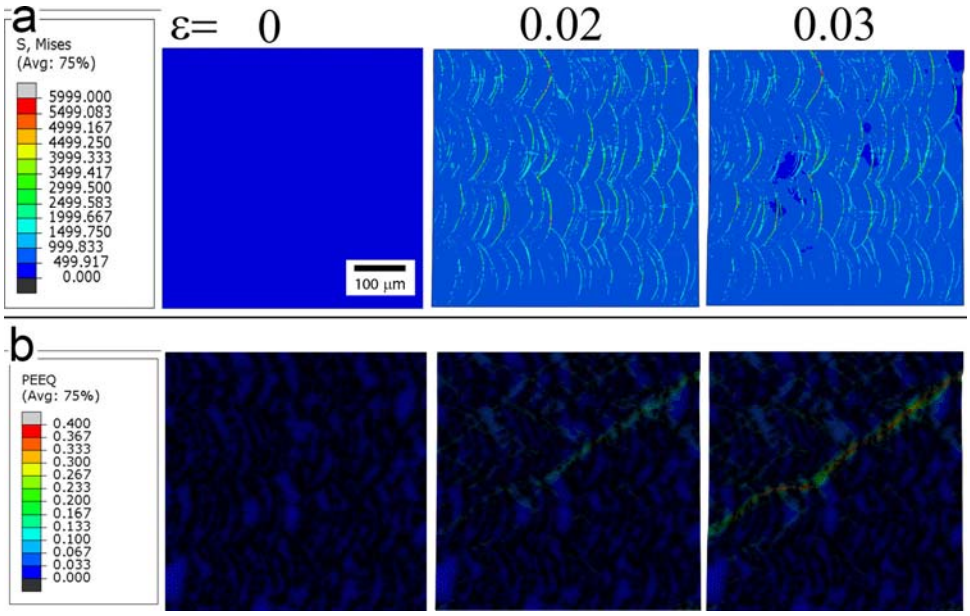

Figure 6. a) Misses stresses and b) Equivalent plastic strain (PEEQ) on the microstructure of vertical specimen at a strain of 0, 0.02, and 0.03

In the case of a parallel specimen, Misses stress and PEEQ strain fields differ more from the vertical specimens (Figure 7). At a strain of 0.02, there is a stress concentration on the fusion boundaries. Upon further loading, the stress concentration on the fusion boundaries is maintained. The straining in the microstructure is distributed homogeneously.

Vertical specimens showed significant strain hardening in the plastic regime. This can be attributed to the localization of the stress flow due to the orientation of the fusion boundaries. Parallel fusion boundaries enhance the strain hardening. However, in the case of vertical specimens, the fusion boundaries significantly hindered stress flow, where boundaries are situated vertically to the loading direction.

The inherent property of the printed microstructure significantly impacts the mechanical properties of the metals and may lead to unexpected results during service.

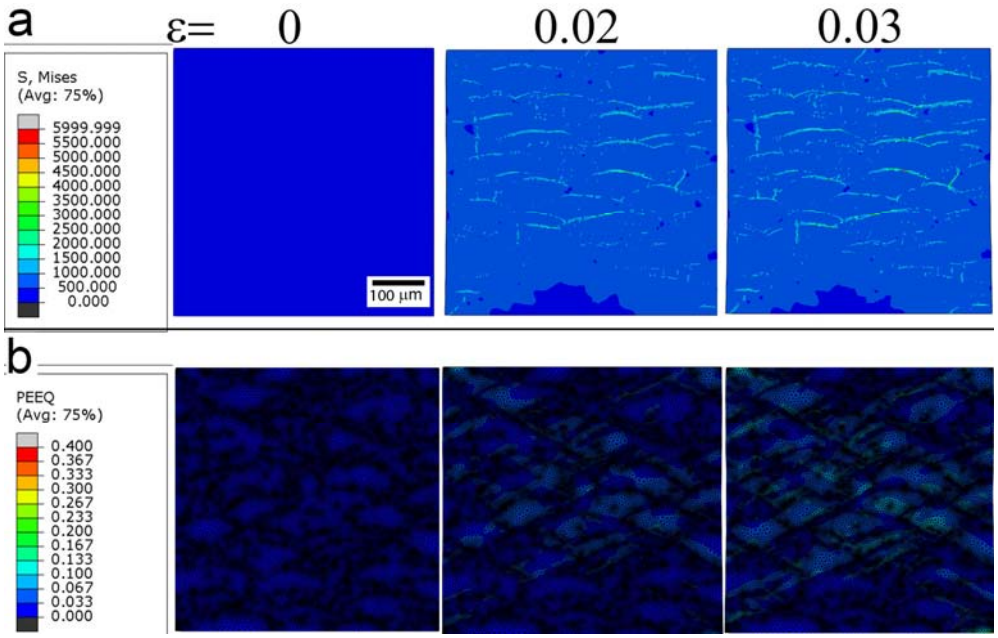

Figure 7. a) Misses stresses and b) Equivalent plastic strain (PEEQ) on the microstructure of parallel specimen at a strain of 0, 0.02, and 0.03

4. CONCLUSIONS

2-D microstructure modeling allows us to demonstrate the influence of the fusion boundary shape and size on the stress and strain distribution in the microstructure. According to findings in this study the following results can be drawn from this study:

1. Parallel built-up specimens possessed larger dimensions and higher amounts of fusion boundaries than vertical specimens.
2. Fusion boundaries are almost parallel to the loading axis for vertically built-up specimens. The enormous strain was localized in the microstructure.
3. Fusion boundaries in parallel specimens are perpendicular to the longitudinal axis, resulting in a more homogenous strain distribution.
4. Higher plasticity of the parallel specimen is due to the uniform distribution of the strain in the microstructure
5. The orientation, size, and amount of the fusion boundaries are important and affect the mechanical properties.

2-D microstructure modeling based on the optical micrographs allows us to analyze the microstructure-property relationship in detail.

5. REFERENCES

1. Kaya, A.C., Salamcı, M.U., Fleck, C., 2023. Influence of anisotropy on the deformation behavior in microtensile 316L steel specimens fabricated by laser powder bed fusion (PBF-LB/M). Materials Science & Engineering A, 863, 144521.

2. Shifeng, W., Shuai, L., Qingsong, W., Yan, C., Sheng, Z., Yusheng, S., 2014. Effect of molten pool boundaries on the mechanical properties of selective laser melting parts. Journal of Materials Processing Technology, 214, 2660-2667.

3. Guan, K., Wang, Z., Gao, M., Li, X., Zeng, X., 2013. Effects of processing parameters on tensile properties of selective laser melted 304 stainless steel. Materials & Design, 50, 581-586.

4. Rehme, O., Emmelmann, C., 2006. Rapid manufacturing of lattice structures with selective laser melting, in: Bachmann, F.G., Hoving, W., Lu, Y., Washio, K., (Eds.), Proc. SPIE 6107, Laser-Based Micropackaging, San Jose, CA, USA, p. 61070K.

5. Güden, M., Yavas, H., Tanrıkulu, A.A., Tasdemirci, A., Akın, B., Enser, S., Karakus, A., Hamat, B.A., 2021. Orientation dependent tensile properties of a selective-laser-melt 316L stainless steel. Materials Science & Engineering A, 824, 141808.

6. Hitzler, L., Hirsch, J., Heine, B., Merkel, M., Hall, W., Ochsner, A., 2017. On the anisotropic mechanical properties of selective laser-melted stainless steel. Materials, 10, 1136.

7. Ahmadi, A., Mirzaeifar, R., Moghaddam, N.S., Turabi, A.S., Karaca, H.E., Elahinia, M., 2016. Effect of manufacturing parameters on mechanical properties of 316L stainless steel parts fabricated by selective laser melting: a computational framework. Materials & Design, 112, 328-338.

8. Rodgers, T.M., Madison, J.D., Tikare, V., 2017. Simulation of metal additive manufacturing microstructures using kinetic Monte Carlo. Computational Materials Science, 135, 78-89.

9. Abramoff, M.D., Magelhaes, P.J., Ram, S.J., 2004, Image processing with Image J Biophoton. Int., 11, 36-42.

10. Ma, J., 2024. Im2mesh (2D image to triangular meshes) (https://www.mathworks.com/matlabcentral/fileexchange/71772-im2mesh-2d-image-to-triangular-meshes), MATLAB Central File Exchange. Retrieved March 23, 2024.

11. Engwirda, D., 2014, Locally-optimal Delaunay-refinement and optimisation-based mesh generation. Ph.D. Thesis, School of Mathematics and Statistics, The University of Sydney, http://hdl.handle.net/2123/13148.

12. Kaya, A.C., 2020. In situ shear behavior of open-cell austenitic 316L steel foams. Materials Chemistry and Physics, 252, 123303.